Supporting Information

Molecular Engineering of Non-Halogenated Solution-Processable Bithiazole based Electron Transport Polymeric Semiconductors

Boyi Fu,[1] Cheng-Yin Wang,[2] Bradley D. Rose,[3] Yundi Jiang,[1] Mincheol Chang,[1] Ping-Hsun Chu,[1] Zhibo Yuan,[4] Canek Fuentes-Hernandez,[2] Bernard Kippelen,[2] Jean-Luc Brédas,[3] David M. Collard,[4] and Elsa Reichmanis[1,4,5*]

[1]School of Chemical & Biomolecular Engineering, Georgia Institute of Technology, 311 Ferst Drive, Atlanta, GA 30332-0100, U.S.A

[2]School of Electrical and Computer Engineering, Georgia Institute of Technology, 777 Atlantic Dr NW, Atlanta, GA 30332-0250, U.S.A

[3]Solar and Photovoltaics Engineering Research Center, King Abdullah University of Science and Technology, Thuwal 23955-6900, Kingdom of Saudi Arabia

[4]School of Chemistry & Biochemistry, Georgia Institute of Technology, 901 Atlantic Drive, Atlanta, GA 30332-0400, U.S.A

[5]School of Materials Science and Engineering, Georgia Institute of Technology, 771 Ferst Drive, Atlanta, GA 30332-0245, U.S.A.

* Corresponding author: ereichmanis@chbe.gatech.edu

Materials and Methods

Chloroform, dichloromethane, toluene, isopropanol, THF, DMF, 2-methoxyethanol, chlorobenzene and 1,2-dichorobenzene (DCB) were purchased as anhydrous grade solvents from Sigma-Aldrich. Mesitylene was purchased from Acros Organics. THF was distilled from sodium benzophenone. 2-Bromothiazole was purchased from Scientific Matrix. Tetrabutylammonium bromide (n-Bu_4NBr), n,n-diisopropylethylamine (DIPEA), diisopropylamine (DIPA), palladium(II) acetate ($Pd(OAc)_2$), tris(dibenzylideneacetone)-dipalladium(0) ($Pd_2(dba)_3$), tri(o-tolyl)phosphine (P(*o*-tolyl)$_3$), sodium diethyldithiocarbmate, polyethylenimine (PEIE, 80% ethoxylated solution, 35 — 40 wt.% in H_2O with *ca*. 70 kDa of Mw), and tetra-*n*-butylammonium hexafluorophosphate ($[n\text{-}Bu_4N]^+[PF_6]^-$) were purchased from Sigma-Aldrich. BCB (XU.71918, Cyclotene^{TM}) was purchased from Dow Chemicals. CYTOP (CTL-809M) and its corresponding solvent (CT-solv.180) were purchased from Asahi Glass, Co. *N*-octadecyltrichlorosilane (OTS-18) was purchased from Gelest, Inc. Silica gel was purchased from Sorbent Technologies (Premium Rf™, porosity: 60Å; particle size: 40-75 μm).

The microwave irridated polymerizations were conducted using a CEM Discover SP System. ^1H and ^{13}C NMR spectra were recorded using a Varian Mercury Vx 400 (^1H, 400 MHz; ^{13}C, 100 MHz) and Vx 300 (^1H, 300 MHz; ^{13}C, 75 MHz) nuclear magnetic resonance spectrometer. Electron ionization mass spectra (EI-MS) were recorded using a Waters AutoSpec. Molecular weights of **PDBTz** were measured using a PL-GPC 220 instrument (courtesy of Ben Cherniawski and Prof. Alejandro L Briseno in the Department of Polymer

Science and Engineering, University of Massachusetts Amherst) using 1,2,4-trichloro-benezene (TCB) as the mobile phase at 135 °C, as shown in **Figure S12**.

UV-vis absorption spectra was recorded on an Agilent 8453 UV-Visible Spectrophotometer. **PDBTz** films for UV-vis absorption characterization were prepared by spin-coating polymer solutions in DCB (5 mg/mL), *o*-xylene (5 mg/mL), *p*-xylene (4 mg/mL), and THN (5 mg/mL) onto OTS-18 pre-treated glass cover substrates. The details of OTS-18 pretreatment are depicted in the section of "OFET Device Fabrication and Characterization" (*vide infra*). Cyclic voltammetry (CV) and differential pulse voltammetry (DPV) were performed using Princeton Applied Research Potentiostat/Galvanostat Model 273A with a three-electrode electrochemical cell consisting of a platinum disk working electrode, onto which polymers were drop casted from DCB solution (1 mg/mL), a platinum flag counter electrode, and a Ag/Ag^+ reference electrode (10 mM of $AgNO_3$ and 0.5 M of Bu_4NPF_6 in acetonitrile). The ferrocene/ferrocenium redox couple (Fc/Fc^+) was used as the internal standard (-5.08 eV versus vacuum).[1] The CV was performed with a scan rate varying from 50 to 200 mV/s for five cycles. DPV parameters were set up as follows: step time 0.038 s, step size of 2 mV, and an amplitude of 100 mV.

Ultraviolet Photoemission Spectra (UPS) were measured on Kratos Axis UltraDLD XPS/UPS system, using He-I lamp radiation at 21.2 eV. All samples were in electronic equilibrium with the spectrometer via a metallic clip on the surface, and were run at a base pressure of 10^{-9} Torr. The Fermi level was calibrated using atomically clean silver. UPS were acquired at 5 eV pass energy and 0.05 eV step size with the aperture and iris set to 55 μm. From

the secondary electron edge (SEE) of the UPS we calculated the work function (ϕ = 21.22-SEE) for each polymer, and from the emission close to the Fermi level we determine the position of valence band maximum. IP (= –HOMO) and ϕ were calculated by equations (1) and (2):

$$\text{IP} = h\nu - (E_{\text{cutoff}} - \varepsilon_V^F) \quad (1)$$

$$\phi = h\nu - E_{\text{cutoff}} \quad (2)$$

where $h\nu$, E_{cutoff}, and ε_V^F denote the incident photo energy (He I, 21.22 eV), the high binding energy cutoff, and the lowest binding energy point, respectively.

The thermal decomposition temperature of polymer was measured with a Perkin-Elmer Pyris 1 thermogravimetric analyzer (TGA) in a nitrogen atmosphere (25 mL min^{-1}) with a heating rate of 10 °C min^{-1}. Thermal transitions of polymer was measured with a TA Q200 Differential Scanning Calorimeter (DSC) in a nitrogen atmosphere (50 mL min^{-1}) with a heating/cooling rate of 10 °C min^{-1}. Each sample was scanned for three cycles.

2D-GIWAXS characterization was carried out using a Bruker-AXS Microdiffractometer (operating voltage of 45 kV and current of 40 mA) with a 0.8 mm collimator, K_α monochromator, Hi-Star area detector, and Eulerian cradle sample holder, at an optimal incidence angle (0.8 — 2° for **PDBTz**), and a 30° out-plane tilt angle. **PDBTz** films for 2D-GIWAXS characterizations were prepared by drop casting **PDBTz** solutions in DCB (5 mg mL^{-1}), *o*-xylene (5 mg mL^{-1}), *p*-xylene (4 mg mL^{-1}), and THN (5 mg mL^{-1}) onto BCB pre-treated SiO_2 dielectric (300 nm) / p^{++} doped Si substrates. The details of BCB pretreatment are depicted in the section of "OFET Device Fabrication and Characterization" (*vide infra*).

The coherence length (τ) of <100> and <010> peaks were calculated based on Scherrer equation:

$$\tau = \frac{K\lambda}{\beta Cos\theta} \quad (3)$$

where K is a dimensionless shape factor (0.9); λ refers to the incidence X-ray wavelength (1.54059 Å in this study); β represents the FWHM (radians) of <100> and <010> peaks along 2θ direction; and θ denotes to Bragg angle.

PDBTz film orientation distribution was investigated by Herman's orientation function (S), as shown in Equation (4) and (5):

$$f = \frac{\int_0^{\pi/2} I(\chi) Cos^2(\chi)\, Sin(\chi) d\chi}{\int_0^{\pi/2} I(\chi)\, Sin(\chi) d\chi} \quad (4)$$

$$S = \tfrac{1}{2}(3f-1) \quad (5)$$

For instance, **Figure S11** shows the <100> and <010> peak distributions along with χ, within a **PDBTz** film cast from *o*-xylene. To simplify the calculation, χ was defined as 0° at the q_z axis (out-of-plane), and as 90° at the q_{xy} axis (in-plane). The $I(\chi)$ term is the <100> or <010> intensity at each χ, and sin(χ) represents a geometric intensity correction factor. The molecular orientation parameter, f, refers to the average lattice plane orientation relative to χ_{max}, the azimuthal angle at which $I(\chi)$ approaches the maximum. According to Equation (4), S = 1, if on average, the lattice planes completely align parallel to χ_{max}; S = -1/2 if they completely orient perpendicular to χ_{max}; while S = 0 if the lattice planes orient randomly.

The surface morphology of **PDBTz** films were characterized by AFM using a Bruker

Dimension Icon Atomic Force Microscope System with ScanAsyst in tapping mode with silicon etched probe tip. Polymer films for AFM characterizations were prepared by spin-coating **PDBTz** solutions in DCB (5 mg mL^{-1}), *o*-xylene (5 mg mL^{-1}), *p*-xylene (4 mg mL^{-1}), and THN (5 mg mL^{-1}) onto BCB pre-treated SiO_2 dielectric (300 nm) / p^{++} doped Si substrates.

The thermal annealing treatments for **PDBTz** films under UV/vis absorption (**Figure S8**), 2D-GIWAXS, and AFM characterizations were implemented on a hotplate with temperature setting at 100 and 150 °C inside a glovebox filled with N_2. Each thermal annealing treatment lasted for 30 min, followed by rapidly cooling to room temperature.

OFET Device Fabrication and Characterization

The BGTC FET devices were fabricated on a heavily p doped silicon wafer <100> as the gate electrode with a 300 nm thick layer of thermally grown SiO_2 as one gate dielectric. BCB pre-diluted in mesitylene with a ratio of 1:20 (v/v) was spin coated onto SiO_2/Si substrates at 3,000 rpm for 1 min. The resulting substrates were annealed at 265 °C for 1.5 h inside a nitrogen-filled glovebox for cross-linking, followed by cooling down to room temperature for 30 min. The BCB/SiO_2 bilayer dielectric has a capacitance of *ca*. 1.04 x 10^{-4} Fm^{-2}. The hot **PDBTz** solutions (4-6 mg mL^{-1}) were subsequently spin-coated (at 1,800 rpm for 1 min) onto BCB/SiO_2 substrates inside glovebox. The spin-coated **PDBTz** based substrates were then annealed at 150 °C for 30 min, followed by rapidly cooling to room temperature. 100 nm of Ca and 150 nm of Al (as a barrier layer to avoid Ca oxidation) were thermally deposited onto

polymer layer in sequence via shadow masks as source and drain electrodes, with channel sizes fixing in width (2 mm) and varying in length (50, 100, 150, and 200 μm). The aluminum layer (150 nm) is attempting to enhance the oxidative stability of the electrodes.

The TGBC OFETs were fabricated based on glass substrates (Corning® 1737). 50 nm of Ag was deposited onto glass substrates as source and drain electrodes via E-beam evaporation, with channel sizes fixing in width (4.5 mm) and varying in length (80, 120, 160, and 200 μm), followed by spin coating (at 5,000 rpm for 1 min, with an acceleration of 1,000 rpm/s) 0.01 or 0.05 wt% of PEIE solution in 2-methoxyethanol. The resultant substrates were annealed at 100 °C for 10 min in a glovebox, affording an ultra-thin PEIE layer with a thickness < 1.5 nm (an exact thickness is not accurate due to the resolution limitation of ellipsometer under 1.5 nm). **PDBTz** solutions were thereafter spin-coated (at 1,800 rpm for 1 min) onto substrates inside glovebox. The spin-coated **PDBTz** based substrates were then annealed at 150 °C for 30 min, followed by rapidly cooling to room temperature. The 2 wt% of CYTOP solution prepared via diluting 9 wt% of CYTOP solution (CTL-809M) by CT-solv. 180 (1: 3.5, v/v) was subsequently spin coated (3,000 rpm for 1 min) onto the polymer layer, followed by a thermal annealing treatment at 100 °C for 20 min in glovebox, to afford a 40 nm of CYTOP layer. A Savannah 100 ALD system from Cambridge Nanotech Inc. was used to deposit 50 nm-thick Al_2O_3 dielectric films[2] Films were grown at 110 °C using alternating exposures of trimethyl aluminum [$Al(CH_3)_3$] and H_2O vapor at a deposition rate of approximately 0.1 nm per cycle. Each deposition cycle (1 ML) lasted 24 s, yielding a total deposition time of around 4 h for 500 cycles. The resultant CYTOP/Al_2O_3 bilayer dielectric has a capacitance of *ca*. 3.18 x 10^{-4} Fm^{-2}. 100 nm of Al gate electrodes were deposited by

thermal evaporation through a shadow mask.

The bottom-gate-bottom-contact (BGBC) FET devices encapsulated by CYTOP (**Scheme S2**) were employed to characterize the air stability of **PDBTz** under 20 °C and 55-65 RH%. BGBC OFETs were fabricated on a heavily p doped silicon wafer <100> as the gate electrode with a 300 nm thick layer of thermally grown SiO_2 as the gate dielectric. Au source and drain contacts (50 nm of Au contacts with 3 nm of Cr as the adhesion layer) with a fixed channel size (50 μm in length and 2 mm in width) were deposited via E-beam evaporator onto the SiO_2 layer using a photolithography lift-off process. Prior to deposition of polymer semiconductors, the devices were cleaned by sonication in acetone for 30 min and subsequently rinsed sequentially with acetone, methanol and isopropanol, followed by drying under a flow of nitrogen. The SiO_2 surface was pretreated by exposing the devices to UV/ozone for 30 min followed by immersion into a 2.54 x 10^{-3} M (1 μL mL^{-1}) solution of OTS-18 in anhydrous toluene overnight inside glovebox. The devices were then cleaned by sonication in toluene for 10 min, followed by rinsing with acetone, methanol and isopropanol, and drying under a flow of nitrogen. The H_2O contact angle for SiO_2 surface after OTS-18 treatment is in the range of 95–105°; while OTS-18 modified SiO_2 dielectric has a capacitance of *ca*. 1.1 x 10^{-4} Fm^{-2}. **PDBTz** solutions were thereafter spin-coated (at 1,800 rpm for 1 min) onto substrates inside glovebox. The spin-coated **PDBTz** based substrates were then annealed at 150 °C for 30 min, followed by rapidly cooling to room temperature. The resultant OFET devices were encapsulated via spin coating 9 wt% of CYTOP solution (at 4,000 rpm for 1 min), followed by a thermal annealing treatment at 100 °C for 20 min in glovebox, to afford a *ca*. 900 nm of CYTOP encapsulation layer. The OFET devices were stored in the ambient condition (25 ^{o}C, 55-65 RH%) and

measured periodically inside glovebox to assess the effect of air on **PDBTz** based device performance (air stability).

The I-V transfer curve of **PDBTz** based on BGBC OFET is shown in **Figure S13**. Due to the high work function of Au (5.1-5.47 eV) that is consistent with the IP of **PDBTz** (5.54 eV), hole transport behavior was observed. The field-effect hole and electron mobilities based on BGBC OFET substrates were approximately at 0.01-0.03 $cm^2V^{-1}s^{-1}$ and 0.15-0.25 $cm^2V^{-1}s^{-1}$, respectively.

The capacitances of the dielectric layers were measured via Agilent 4284A Precision LCR Meter. For BCB/SiO_2 bilayer dielectric, a parallel-plate capacitor was fabricated on a heavily p doped silicon wafer <100> as one electrode with a 300 nm thick layer of thermally grown SiO_2. BCB layer was afforded using the identical method in BGTC OFET device fabrication (*vide supra*). 150 nm of Al were thermally deposited onto polymer layer in sequence via shadow masks as the 2nd electrode. For OTS-18/SiO_2 dielectric, the capacitor was fabricated on a heavily p doped silicon wafer <100> as one electrode with a 300 nm thick layer of thermally grown SiO_2. OTS-18 was grown onto the SiO_2 substrate using the identical method in BGBC OFET device fabrication (*vide supra*). 150 nm of Al were thermally deposited onto polymer layer in sequence via shadow masks as the 2nd electrode.

All OFET characterizations were performed using a probe station inside a nitrogen filled glovebox using an Agilent 4155C (for BGTC and BGBC OFETs) or Agilent E5272A (for TGBC OFETs) semiconductor parameter analyzers. The FET mobilities were calculated from the saturation regime (V_{SD} = 80 V in BGTC and BGBC OFETs, and V_{SD} = 10 V in TGBC

OFETs) in the transfer plots of V_G versus I_{SD} by extracting the slope of the linear range of V_G vs. $I_{SD}^{1/2}$ plot and using the following equation:

$$\left.\frac{\partial I_{SD}^{1/2}}{\partial V_G}\right|_{V_{SD}} = \left(\mu_h C_{ox}(\frac{W}{2L})\right)^{1/2}$$

where I_{SD} and V_{SD} are the source-drain current (A) and source-drain voltage (V), respectively; V_G is the gate voltage (V) scanning from -20 to 80 V (for BGTC and BGBC OFETs) or 0 to 16 V (for TGBC OFETs) in the transfer plot; C_{ox} is the capacitance per unit area of the gate dielectric layer. W and L refer to the channel length and width; μ_e represents the electron field-effect mobility in the saturation regime ($cm^2V^{-1}s^{-1}$).

In this study, the threshold voltage, V_{th}, was calculated by extrapolating $V_T = V_G$ at $I_{SD} = 0$ in the V_G vs. $I_{SD}^{1/2}$ curve. Current on and off ratio, $I_{ON/OFF}$, was determined through dividing maximum I_{SD} (I_{ON}) by the minimum I_{SD} at around V_G in the range of -40 to 0 V (I_{OFF}).

It is noted that **PDBTz** field-effect mobility was more stable and hysteresis was reduced after thermal annealing at 150 °C for 30 min in OFETs and no obvious improvement was observed at annealing temperatures above 150 °C. The thermal annealing treatment was hence fixed at 150 °C for 30 min.

Hansen Solubility Parameter Characterization

PDBTz (1.5 mg) was mixed with 0.3 and/or 1.5 mL of solvent as per the defined procedure for solubility parameter determination and heated at 60 □C for at least 1 h.[3]

Solutions were cooled to ambient temperature where they remained for 12 h. The solubility parameters were determined from these solutions via visual examination. Solvents were categorized as poor if they were unable to dissolve more than 5 mg of **PDBTz**/mL of solvent and good if they were able to dissolve more than 5 mg of **PDBTz**/mL of solvent. For the purposes of Hansen solubility parameter (HSP) analysis using requisite software (Hansen Solubility Parameters in Practice 3rd edition), a poor solvent was assigned a value of "0" and good solvent was assigned a value of "1".

DFT Studies of PDBTz and PDQT Oligomers and Their Subunits

A DFT study of the building blocks for **PDBTz** and PDQT was performed, to explore the effect of bithiazole on polymer conformation and molecular orbitals. Popular DFT methods, such as B3LYP, suffer from delocalization error, *i.e.*, they tend to overly delocalize the electron density. As a result, properties such as torsion barriers and molecular orbital distributions can be poorly described when studying highly conjugated systems. Therefore, we rely here on a long-range corrected hybrid functional, ωB97X, with the cc-pVDZ basis set.[4]

The standard ωB97X functional has been shown to accurately reproduce torsion potentials for bithiophene.[5] The range separation parameter ω ($bohr^{-1}$) determines where the electron exchange description changes from DFT (in the short range) to Hartree-Fock (in the long range), according to:

$$\frac{1}{r} = \frac{1 - \mathrm{erf}(\omega r)}{r} + \frac{erf(\omega r)}{r}$$

where erf represents the error function.

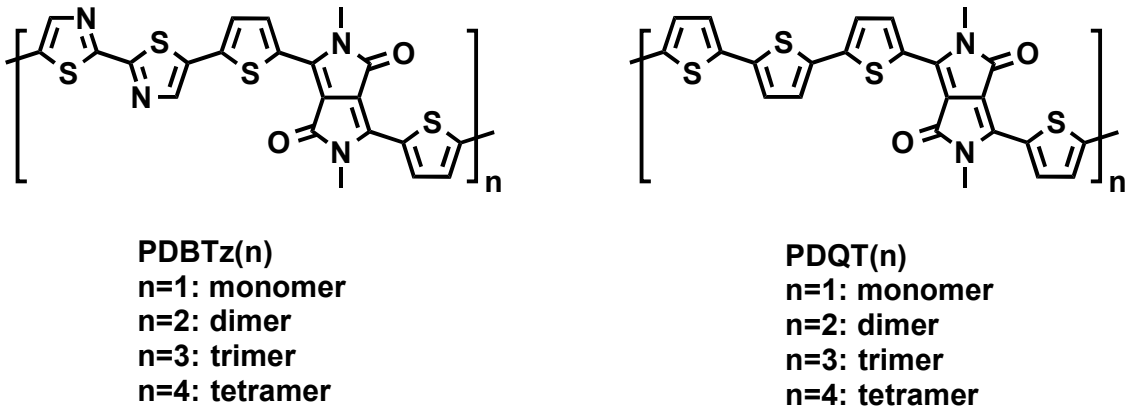

Figure S1. Monomer, dimer, trimer, and tetramer of **PDBTz** and PDQT investigated at the DFT level. Side chains were defined as methyl group to simplify the DFT calculation.

The optimum ω-value has been shown to vary with the conjugation length of the system; thus, the use of the default ω-value would yield an improper description of the (de)localization effects.[6] The range separation parameter ω was optimized for the system following the fundamental-gap tuning procedure:[7]

$$J_{IP}(\omega) = \left|\varepsilon^{\omega}_{HOMO}(N) + E^{\omega}_{gs}(N-1) - E^{\omega}_{gs}(N)\right|$$

$$J_{EA}(\omega) = \left|\varepsilon^{\omega}_{HOMO}(N+1) + E^{\omega}_{gs}(N) - E^{\omega}_{gs}(N+1)\right|$$

$$J_{gap}(\omega) = \sqrt{\left(J_{IP}(\omega)\right)^2 + \left(J_{EA}(\omega)\right)^2}$$

In this procedure $\varepsilon^{\omega}_{HOMO}(N)$ and $\varepsilon^{\omega}_{HOMO}(N+1)$ are the HOMO energies for an N (neutral) and N+1 (anionic) electron system. $E^{\omega}_{gs}(N-1)$, $E^{\omega}_{gs}(N)$, and $E^{\omega}_{gs}(N+1)$ are the total energies for the N-1 (cationic), N (neutral) and N+1 (anionic) electron systems. The ω-value is varied until the minimum value of $J_{gap}(\omega)$ is found. Although the basis set used

in the tuning process may be of initial concern, especially since the tuning procedure involves calculations of the anion with a basis set lacking diffuse functions, it has previously been established that the results from the ω tuning procedure change a trivial amount upon using basis sets larger than the one we are considering.[8] Nonetheless the basis set effects were explored for the model case of bithiophene where the tuned ω parameter using the larger aug-cc-pVTZ basis set was identical to that obtained with the smaller cc-pVDZ basis set. As has been consistently the case in earlier studies of highly conjugated systems using various functionals, the tuned ω-values are found to be smaller than the ωB97X default ω-value of 0.3 $bohr^{-1}$.[6] This holds true even in bithiophene that is the smallest conjugated building block considered (**Table S1**).

Table S1. Tuned ω for systems using tuned-ωB97X/cc-pVDZ// tuned-ωB97X/cc-pVDZ.

compound	ω ($bohr^{-1}$)	ω ($bohr^{-1}$) using aug-cc-pVTZ
bithiophene	0.221	0.221
bithiazole	0.237	---
1	0.195	---
thiothiazole	0.226	---
PDBTz1	0.143	---
PDBTz2	0.115	---
PDBTz3	0.106	---
PDPPT41	0.142	---
PDPPT42	0.112	---
PDPPT43	0.103	---

The torsional potentials of the subunits were tested with the tuned-ωB97X functional, as the standard ωB97X functional was shown to give accurate torsional potentials when compared with benchmark calculations.[5] Tuned-ωB97X predicts bithiophene to have an

optimized S-C-C-S dihedral angle of 152° in comparison to 148° measured by gas phase electron diffraction,[4d] 156° for MP2/aug-cc-pVTZ calculations,[5] which lends confidence that the methodology we use is appropriate for determining this torsion. The tuned-ωB97X energies were also compared to spin component scaled second order Møller–Plesset (SCS-MP2) results using the cc-pVTZ basis set, as this method is expected to produce reliable results to serve as a benchmark.[9] The torsional space of the other interactions were explored to determine the preferred conformational orientations of the polymer building blocks (**Figure 1**). The torsions angle is determined by S-C-C-S for bithiophene and bithiazole while S-C-C-N determined the dihedral angle for **1** (**Figure 1**). Tuned-ωB97X predicts the torsional potential of bithiazole to be about 1.4 kcal/mol less at the *trans*-co-planar orientation relative to the approximately 150° dihedral angle found in bithiophene. In the case of **1**, tuned-ωB97X overestimated the rotational barrier height by about 2 kcal/mol with respect to SCS-MP2, but still yields the correct minimum energy dihedral angle.

The frontier molecular orbital distributions and energies of bithiophene and bithiazole were compared (**Figure S2**). Examination reveals a rather small difference in the HOMO and LUMO wavefunction characteristics between bithiazole and bithiophene. The HOMO-LUMO energy gaps are similar for both bithiazole (8.34 eV) and bithiophene (8.27 eV); as expected, the HOMO and LUMO energies are more stabilized in bithiazole, by about 0.65 eV.

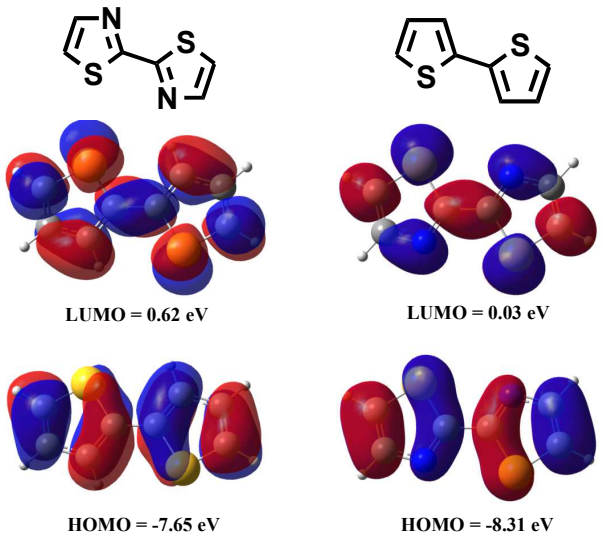

Figure S2. Plots of the frontier molecular orbitals for bithiophene (left) and bithiazole (right) using an isovalue of 0.02. Eigenvalues are shown below the respective orbital.

We considered oligomers up to the tetramer to represent the polymers. The HOMO-LUMO energy gap is predicted to be essentially identical for the monomer units, 4.76 eV for **PDBTz(1)** and 4.76 eV for PDQT(1). This trend continues for the other **PDBTz** and PDQT oligomers studied. The S-C-C-S dihedral angles for the bithiazole and bithiophene units are 180° and 155° for **PDBTz(1)** and PDQT(1) respectively, illustrating the increased planarity of the (isolated) **PDBTz(1)** monomer units. In the longer systems. the S-C-C-S dihedral angle for the bithiazole units in **PDBTz(4)** remains 180° while bithiophene in PDQT(4) varies from 155° to 168°.

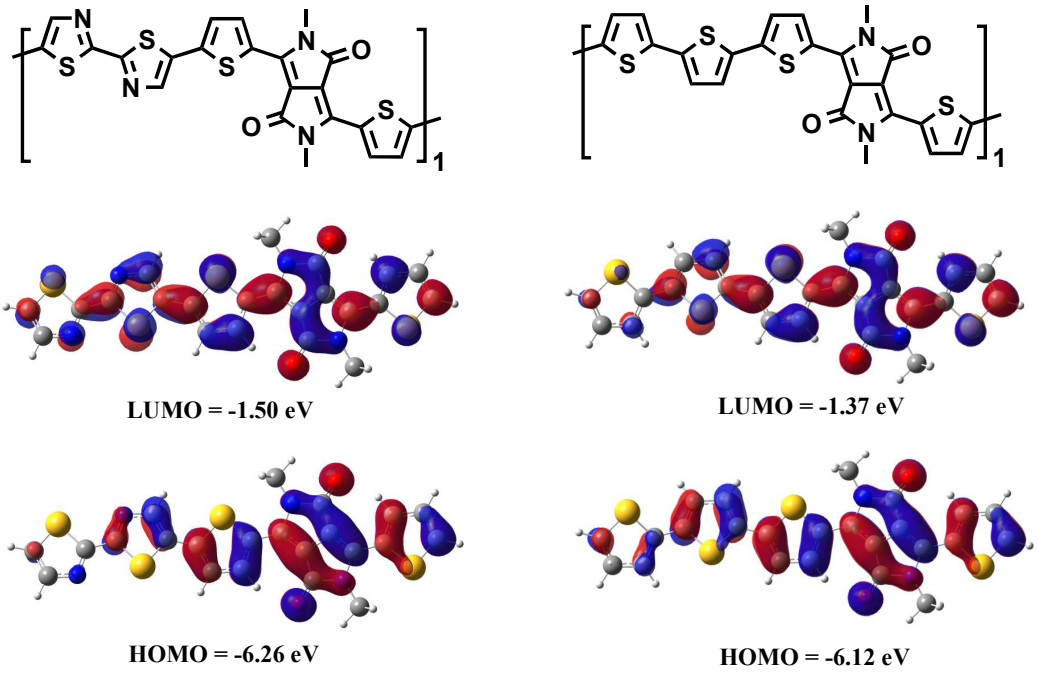

Figure S3. Plots of the frontier molecular orbitals for **PDBTz(1)** (left) and PDQT(1) (right) using an isovalue of 0.02. Eigenvalues are shown below the respective orbital.

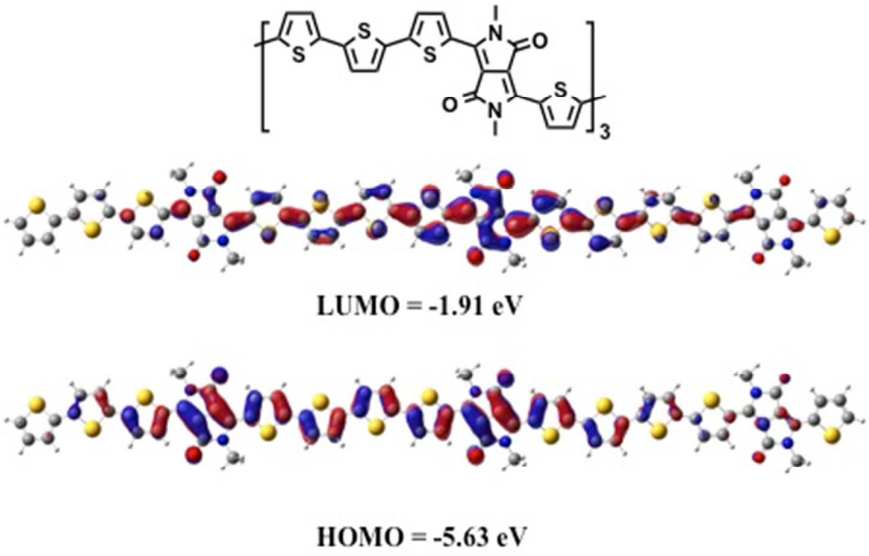

Figure S4a. Plots of the frontier molecular orbitals for PDQT(3) using an isovalue of 0.02. Eigenvalues are shown below the respective orbital.

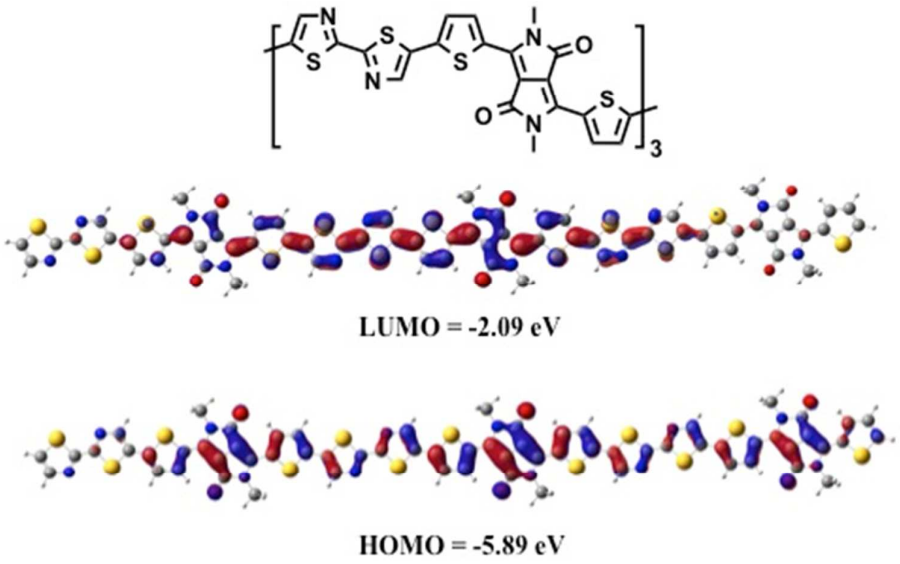

Figure S4b. Plots of the frontier molecular orbitals for **PDBTz(3)** using an isovalue of 0.02. Eigenvalues are shown below the respective orbital.

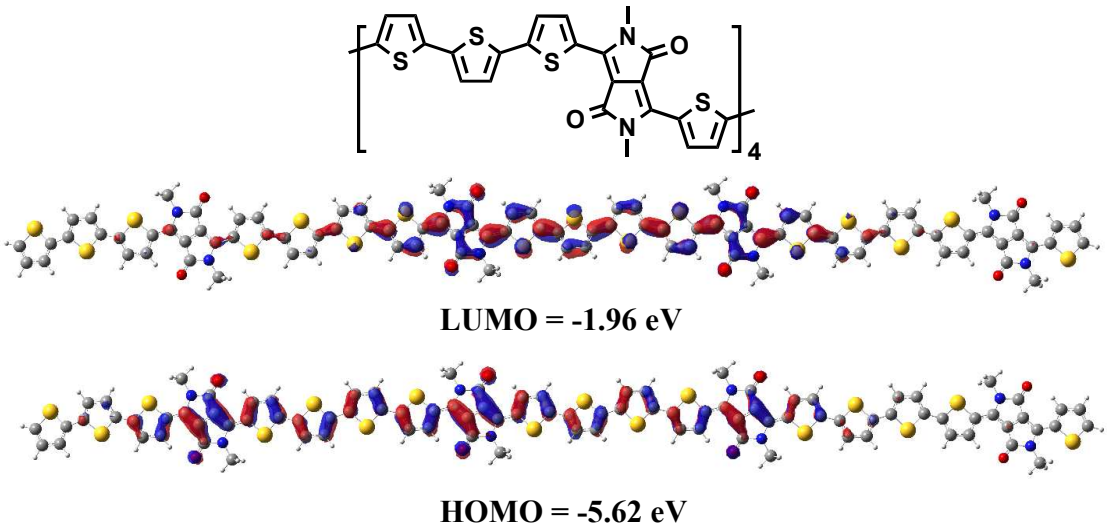

Figure S5a. Plots of the frontier molecular orbitals for PDQT(4) using an isovalue of 0.02. Eigenvalues are shown below the respective orbital.

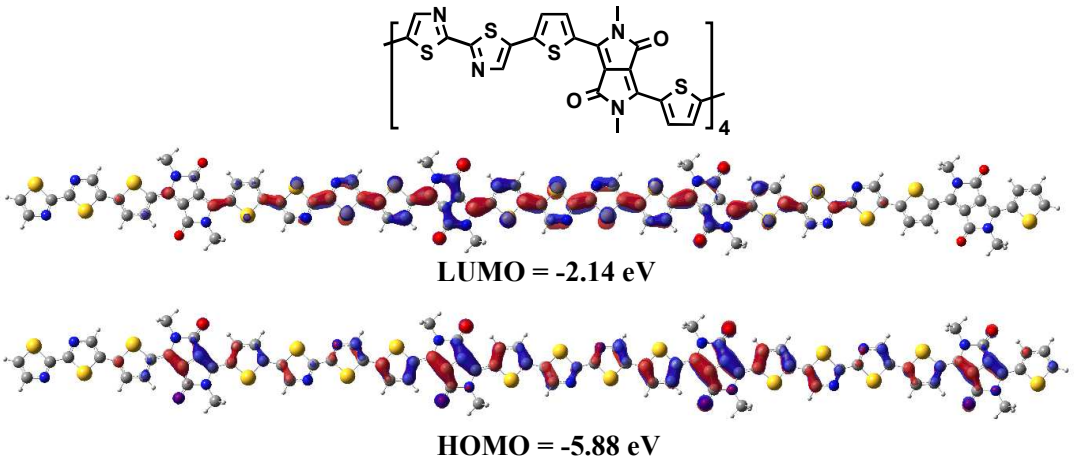

Figure S5b. Plots of the frontier molecular orbitals for **PDBTz(4)** using an isovalue of 0.02. Eigenvalues are shown below the respective orbital.

A reasonable starting geometry was generated using ωB97X/cc-pVDZ. Then the ω-value for this functional was tuned using the fundamental-gap tuning method (*vide supra*). The geometry was re-optimized using the newly tuned ω-value with the same method. The process of tuning the ω-value and re-optimizing the geometry was repeated until the change in the ω-value was less than 1×10^{-3} $bohr^{-1}$. In the case of calculating torsional potentials, the tuned ω-value for the optimized geometry was used for all dihedral angles. The dihedral angles were varied from 0° to 180° in increments of 5°.

Table S2. HOMO and LUMO energies and HOMO-LUMO energy gaps.

molecule	HOMO (eV)	LUMO (eV)	HOMO-LUMO Gap (eV)
bithiophene	-7.65	0.62	8.27
bithiazole	-8.31	0.03	8.34
$PDBTz_1$	-6.26	-1.50	4.76
$PDBTz_2$	-5.97	-1.96	4.01
$PDBTz_3$	-5.89	-2.09	3.79
$PDBTz_4$	-5.88	-2.14	3.73
$PDQT_1$	-6.12	-1.37	4.75
$PDQT_2$	-5.74	-1.77	3.97
$PDQT_3$	-5.63	-1.91	3.71
$PDQT_4$	-5.62	-1.96	3.66

Synthetic Details

The synthetic procedures for the preparation of 2,2'-bithizole (**1**), 5,5'-bis(trimethyl-stannyl)-2,2'-bithiazole (**2**), and 2,5-bis(5-decylheptadecyl)-3,6-di(thiophen-2-yl)pyrrolo[3,4-c]pyrrole-1,4(2H,5H)-dione (**M1**) were modified from published literatures.[10]

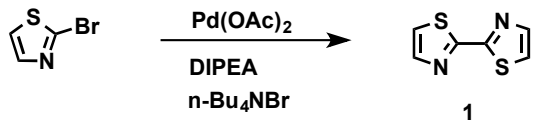

1

2,2'-bithiazole (1): 2-bromothiazole (2.00 g, 12.20 mmol, 1.00 eq.), n,n-diisopropylethyl-amine (DIPEA, 2.13 mL, 12.20 mmol, 1.00 eq.), n-Bu_4NBr (1.97 g, 6.10 mmol, 0.50 eq.), and $Pd(OAc)_2$ (0.14 g, 0.61 mmol, 0.05 eq.) were dissolved into toluene (33.3 mL) under argon. The mixture was heated at reflux overnight, before cooling to room temperature. D.I. H_2O (100 mL) was added and the mixture was extracted into dichloromethane (50 mL). The organic solution was washed with brine (4x50 mL), dried over anhydrous MgSO4, and concentrated under reduced pressure. The resultant dark residue was purified by column chromatography (silica gel, hexane/DCM, 1:8 v/v), followed by recrystallization from heptane to afford 2,2'-bithiazole as needle-like pale yellow crystals (yield: 60%). ^{1}H NMR (300 MHz, $CDCl_3$) δ 7.90 (d, J = 3.1, 2H), 7.44 (d, J = 3.1, 2H). ^{13}C NMR (75 MHz, $CDCl_3$) δ 161.32, 139.98, 135.23, 130.58, 129.77, 128.57, 107.68, 42.26, 37.29, 33.55, 33.27, 30.35, 30.13, 29.71, 29.65, 29.35, 26.66, 24.04, 22.68, 14.10. EI- MS (m/z): 168.0 [M].

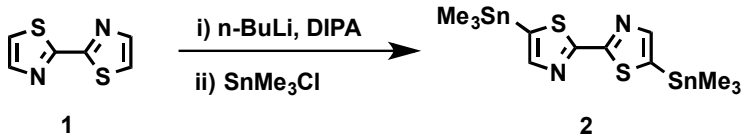

1 2

5,5'-bis(trimethylstannyl)-2,2'-bithiazole (2): DIPA (0.45 mL, 3.12 mmol, 3.50 eq.) in THF (2 mL) was cooled to -78 ˚C under argon, followed by the dropwise addition of n-butyllithium (1.00 mL of a 2.5 M solution in hexane, 2.50 mmol, 2.80 eq.). The resulting solution was stirred at 0 ℃ for 30 min to afford lithium diisopropylamide (LDA). It was subsequently cooled down to -78 ˚C. Compound **1** (150 mg, 0.9 mmol, 1.00 eq.) in THF (3.9 mL) was added in a dropwise manner generating an orange solution. After stirring at -78 ˚C for 2 h, $SnMe_3Cl$ (3.25 mL of a 1.0 M solution in THF, 3.25 mmol, 3.64 eq.) was added in a dropwise manner. The resulting solution was then warmed to room temperature and stirred for 12 h. After poured into D.I. H_2O (50 mL), the mixture was extracted into CH_2Cl_2 (3 x 15 mL), washed with brine (3 x 15 mL), dried over anhydrous $MgSO_4$, and concentrated under reduced pressure. The final product was washed with hexane at -78 ˚C and isolated compound **2** as a pale yellow solid (370 mg, yield: 85%). ^1H NMR (300 MHz, $CDCl_3$) δ 7.77 (s, 2 H), 0.41 (s, 18H).

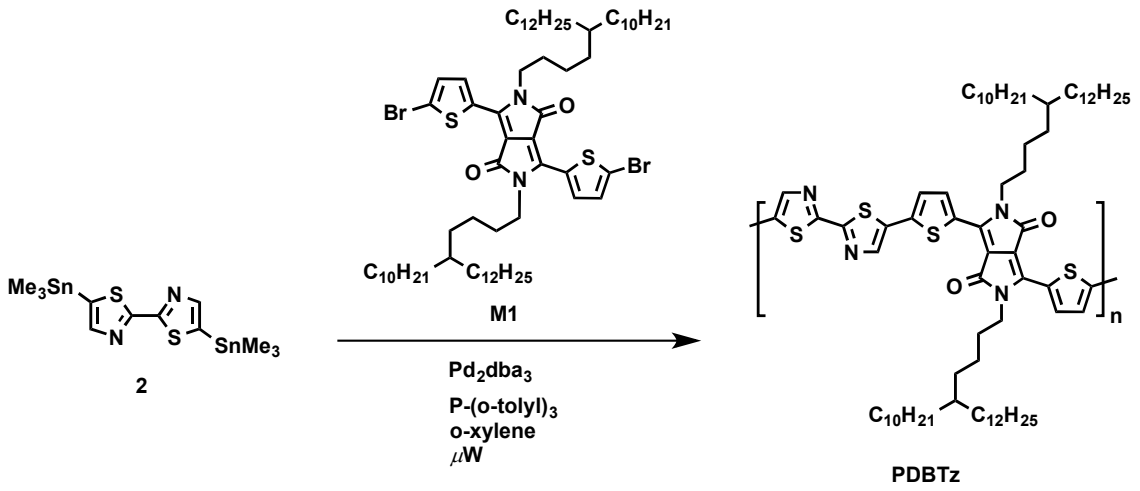

Poly(dithienyl-diketopyrrolopyrrole-dithiazole) (PDBTz): Monomers **2** (60 mg, 0.12 mmol, 1.00 eq.) and **M1** (148 mg, 0.12 mmol, 1.00 eq.), and P(o-tolyl)$_3$ (14.8 mg, 0.05 mmol, 0.40 eq.), were placed in a microwave irradiation tube (10 mL). $Pd_2(dba)_3$ (4.5 mg, 4 μmol, 0.04 eq.) was added and the irradiation tube was then degassed and refilled with argon in sequence. *o*-Xylene (1.05 mL) was added, followed by a 3 cycles of freeze-pump-thaw. The resulting mixture was stirred at 160 °C under microwave irradiation for 1.5 h. The resulting dark gel like crude product was dispersed in chloroform (20 mL) and the solution was poured into aqueous sodium diethyldithiocarbmate solution (100 mL of a solution containing 1g in 100 mL of D.I. water). The resulting mixture was stirred at 75 °C for 2 h to remove Pd. The organic solution was collected and concentrated under reduced pressure. The concentrated solution was added dropwise to methanol (300 mL). The precipitated solid was collected by filtration and purified by Soxhlet extraction sequentially using methanol (24 h), acetone (24 h), ethyl acetate (12 h), hexane (24 h), and $CHCl_3$ (2 h). The $CHCl_3$ solution was collected and then concentrated under reduced pressure. The concentrated solution was added in a dropwise manner to methanol (200 mL). The precipitate was collected by filtration and dried

under vacuum at room temperature for 12 h to afford **PDBTz** as a black solid (145 mg, yield: 90%). Elemental analysis. Calculated for $C_{74}H_{116}N_4O_2S_4$: C, 72.73 %; H, 9.57 %; N, 4.58 %; S, 10.50 %. Found: C, 72.54 %; H, 9.44 %; N, 4.53 %; S, 10.35 %.

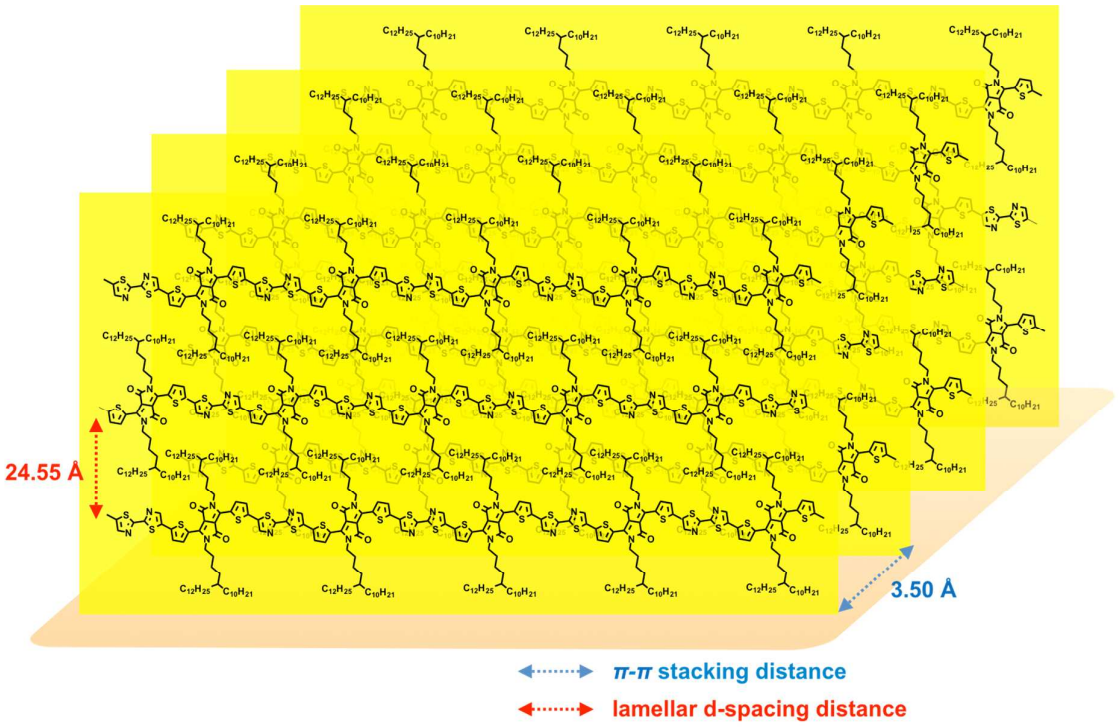

Scheme S1. The estimated lamellar structured edge-on orientation of **PDBTz** on substrate. The alkyl side chain packing of **PDBTz** follows the interdigitated packing model.

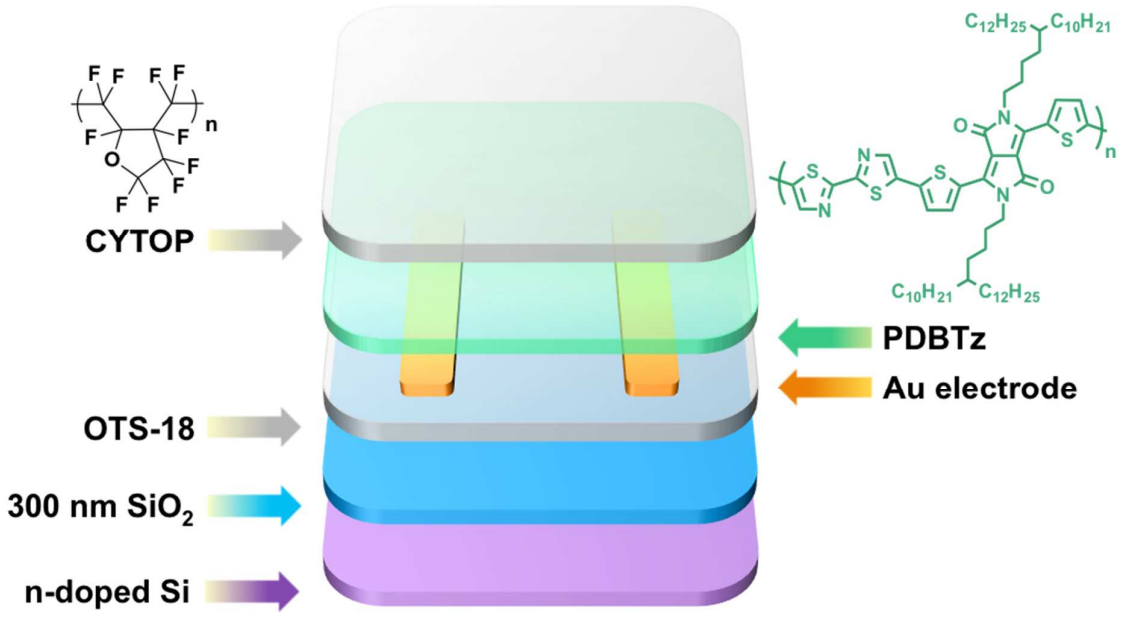

Scheme S2. The architecture of **PDBTz** based bottom-gate/bottom-contact OFET devices encapsulated via a *ca*. 900 nm of CYTOP layer.

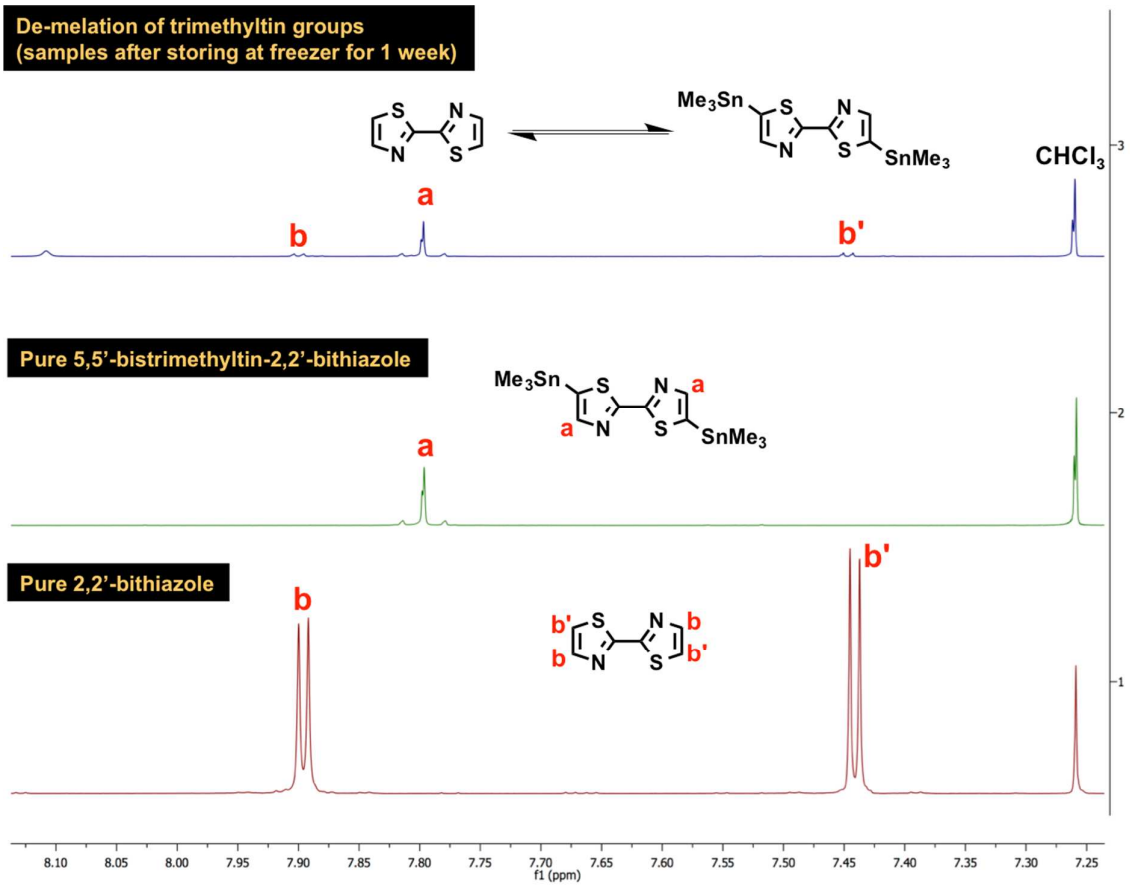

Figure S6. The ^{1}H-NMR results of pure 2,2'-thiazole, 5,5'-bistrimethyltin-2,2'-bithiazole, and de-metalation of 5,5'-bistrimethyltin-2,2'-bithiazole after samples stored at freezer for 1 week.

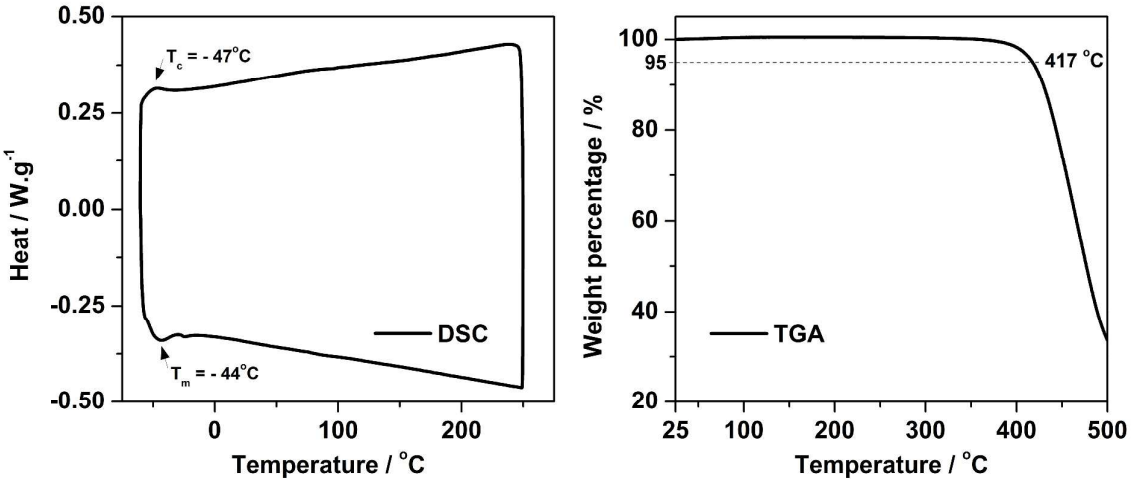

Figure S7. Left: thermal transition characterization of **PDBTz** under DSC. All DSC characterizations were based on the 2nd heating and cooling processes in a nitrogen atmosphere with a nitrogen flow rate of 50 mL/min and a heating/cooling rate of 10 °C/min. Right: TGA of **PDBTz** in a nitrogen atmosphere (25 mL min^{-1}) at a heating rate of 10 °C min^{-1}.

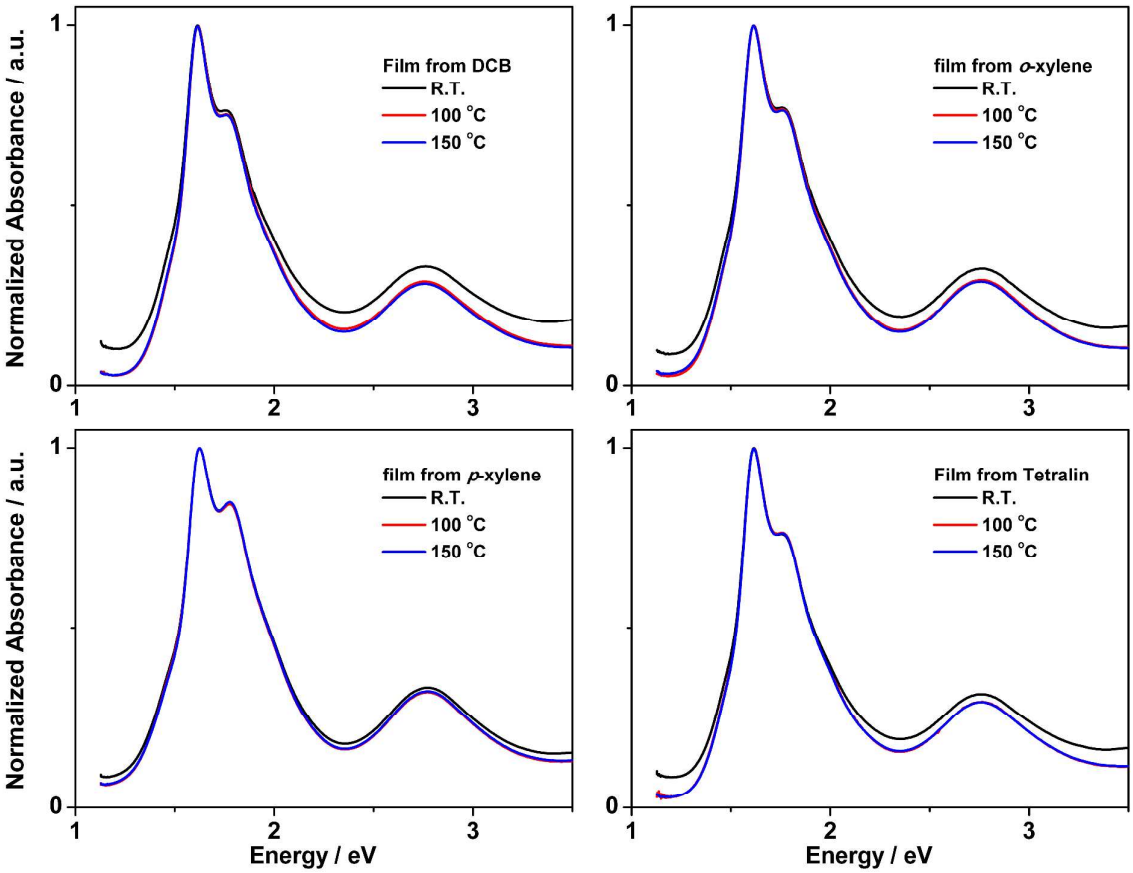

Figure S8. Absorption spectra of **PDBTz** thin films cast from DCB, *o*-xylene, *p*-xylene, and tetralin at room temperature and after thermal annealing treatment under 100 and 150 °C for 30 min followed by cooling down to room temperature.

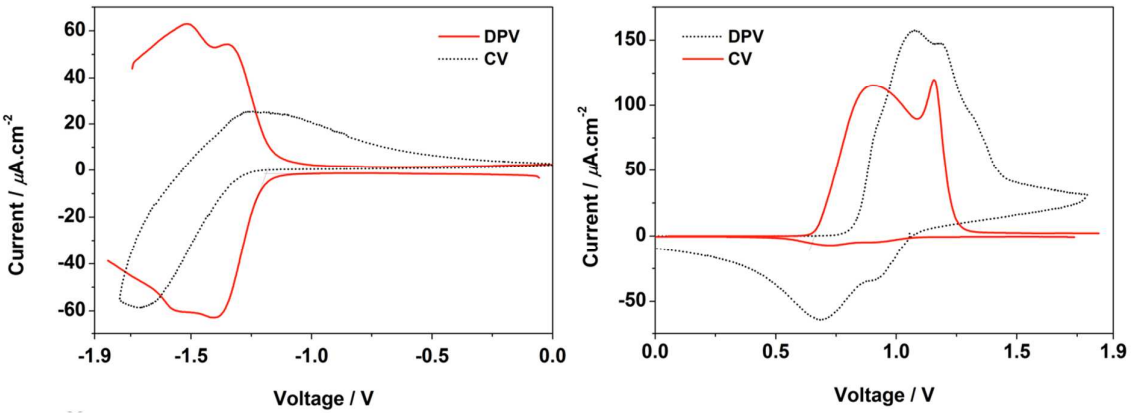

Figure S9. Electrochemical characterizations of **PDBTz** films under cyclic voltammetry (CV) and differential pulse voltammetry (DPV).

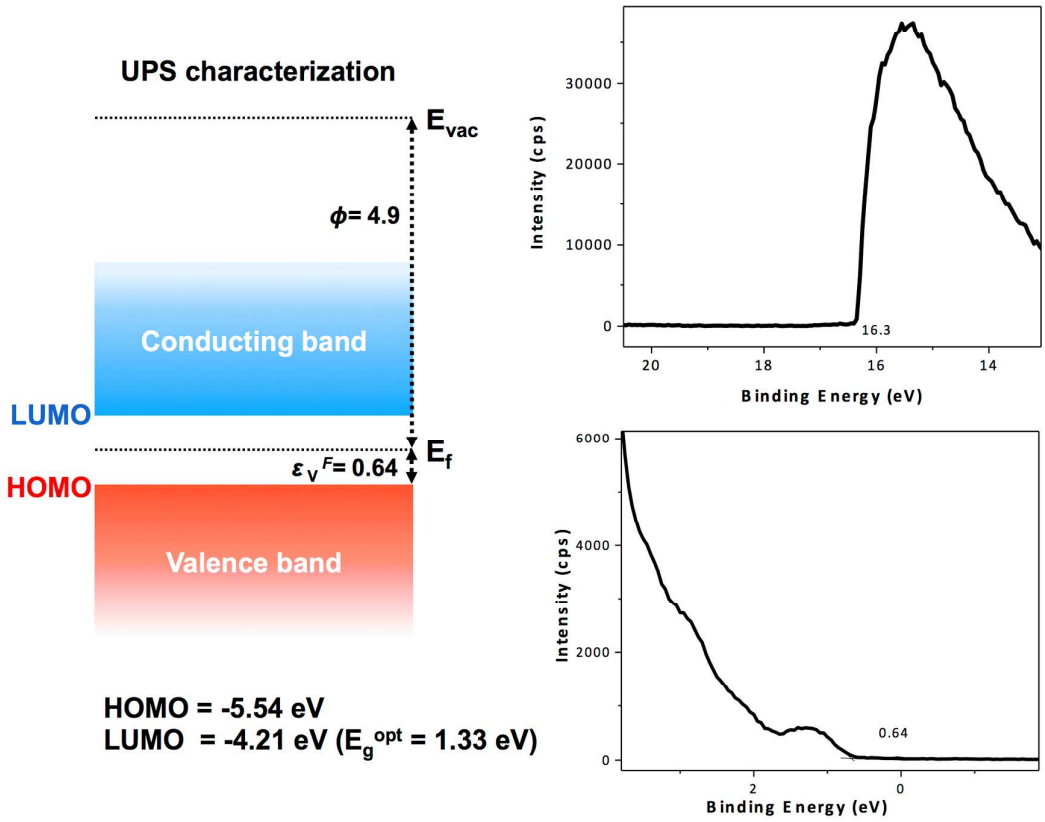

Figure S10. UPS characterization of **PDBTz** thin-films after thermal annealing treatment at 150 ℃ for 30 min.

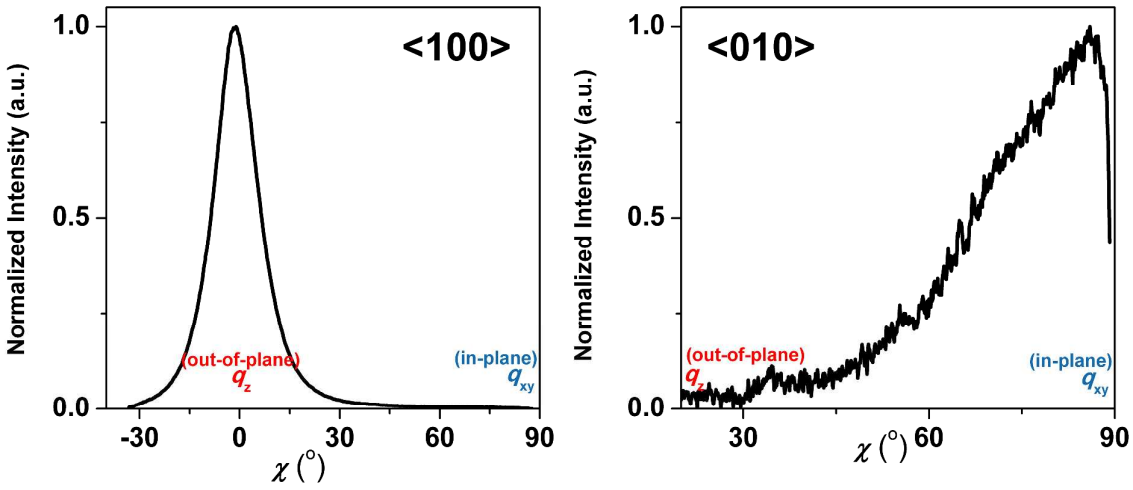

Figure S11. The intensity distribution of the <010> and <010> peaks of **PDBTz** films along the χ axis from q_z (out-of-plane, $\chi = 0°$) to q_{xy} (in-plane, $\chi = 90°$).

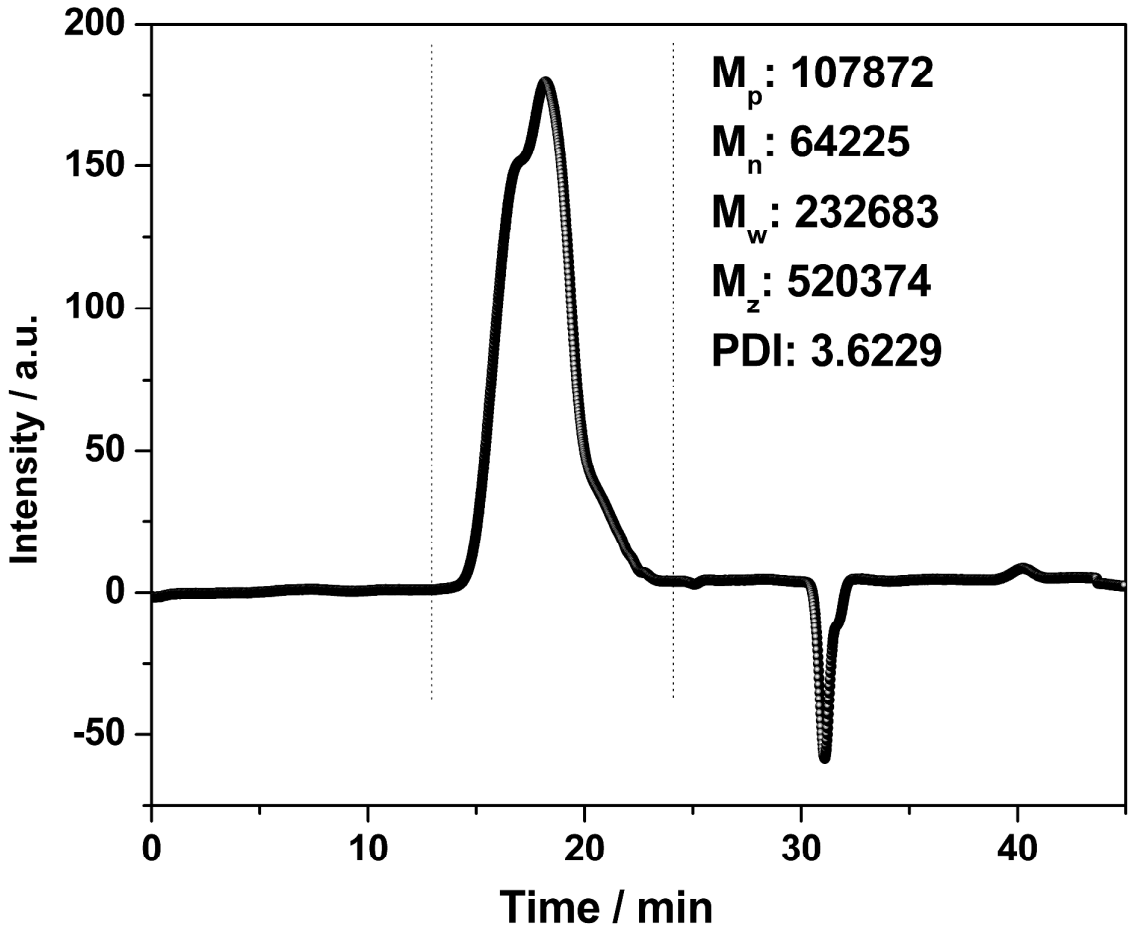

Figure S12. GPC characterization of **PDBTz** using TCB as the mobile phase at 135 °C

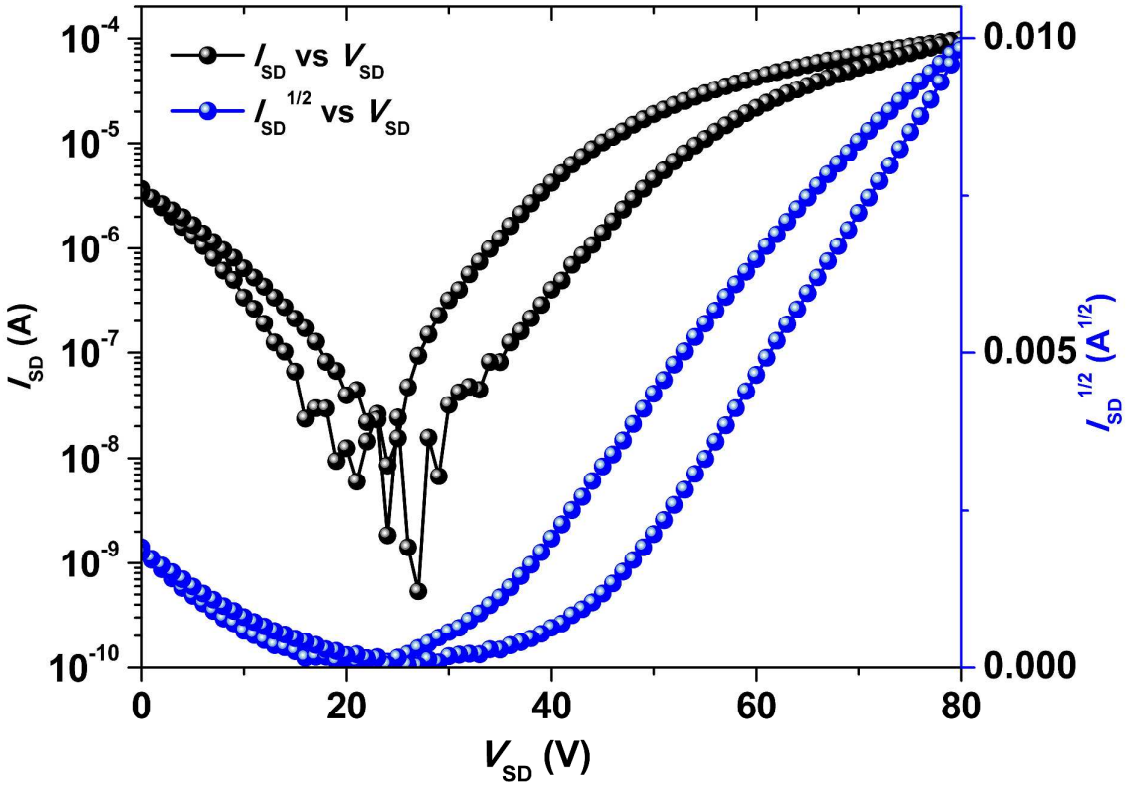

Figure S13. I-V transfer curve of **PDBTz**-based OFETs with bottom-gate/bottom-contact architecture.

Reference

[1] a) C. M. Cardona, W. Li, A. E. Kaifer, D. Stockdale, G. C. Bazan, *Adv. Mater.* **2011**, *23*, 2367; b) R. Stalder, J. G. Mei, J. Subbiah, C. Grand, L. A. Estrada, F. So, J. R. Reynolds, *Macromolecules* **2011**, *44*, 6303.

[2] a) X. H. Zhang, B. Domercq, X. D. Wang, S. Yoo, T. Kondo, Z. L. Wang, B. Kippelen, *Org Electron* **2007**, *8*, 718; b) J. B. Kim, C. Fuentes-Hernandez, W. J. Potscavage, X. H. Zhang, B. Kippelen, *Appl Phys Lett* **2009**, *94*.

[3] M. Chang, D. Choi, B. Fu, E. Reichmanis, *ACS Nano* **2013**, *7*, 5402.

[4] a) J. D. Chai, M. Head-Gordon, *J. Chem. Phys.* **2008**, *128*; b) T. H. Dunning, *The Journal of Chemical Physics* **1989**, *90*, 1007; c) D. E. Woon, T. H. Dunning, *The Journal of Chemical Physics* **1993**, *98*, 1358; d) S. Samdal, E. J. Samuelsen, H. V. Volden, *Synth. Met.* **1993**, *59*, 259; e) C. Quattrocchi, R. Lazzaroni, J. L. Bredas, *Chem. Phys. Lett.* **1993**, *208*, 120; f) A. A. Mohamed, *Int. J. Quantum Chem.* **2000**, *79*, 367.

[5] J. W. G. Bloom, S. E. Wheeler, *J. Chem. Theory Comput.* **2014**, *10*, 3647.

[6] T. Körzdörfer, J.-L. Brédas, *Acc. Chem. Res.* **2014**, *47*, 3284.

[7] a) L. Kronik, T. Stein, S. Refaely-Abramson, R. Baer, *J. Chem. Theory Comput.* **2012**, *8*, 1515; b) N. Kuritz, T. Stein, R. Baer, L. Kronik, *J. Chem. Theory Comput.* **2011**, *7*, 2408; c) R. Baer, E. Livshits, U. Salzner, *Annual Review of Physical Chemistry, Vol 61* **2010**, *61*, 85; d) I. T. Lima, C. Risko, S. G. Aziz, D. A. da Silva Filho, J.-L. Bredas, *J Mater Chem C* **2014**, *2*, 8873.

[8] a) C. Sutton, T. Korzdorfer, M. T. Gray, M. Brunsfeld, R. M. Parrish, C. D. Sherrill, J. S. Sears, J. L. Bredas, *J. Chem. Phys.* **2014**, *140*; b) H. T. Sun, J. Autschbach, *J. Chem. Theory Comput.* **2014**, *10*, 1035.

[9] K. E. Riley, J. A. Platts, J. Rezac, P. Hobza, J. G. Hill, *J. Phys. Chem. A* **2012**, *116*, 4159.

[10] a) M. Lemaire, J. Hassan, L. Lavenot, C. Gozzi, *Tetrahedron Lett.* **1999**, *40*, 857; b) M. O. Wolf, M. S. Wrighton, *Chem. Mater.* **1994**, *6*, 1526; c) B. Y. Fu, J. Baltazar, A. R. Sankar, P. H. Chu, S. Y. Zhang, D. M. Collard, E. Reichmanis, *Adv. Funct. Mater.* **2014**, *24*, 3734.